Hindawi Publishing Corporation
Advances in Materials Science and Engineering
Volume 2014, Article ID 491930, 14 pages
http://dx.doi.org/10.1155/2014/491930

Research Article

Numerical Simulation Procedure for Modeling TGO Crack Propagation and TGO Growth in Thermal Barrier Coatings upon Thermal-Mechanical Cycling

Ding Jun,[1,2] Huang Xia,[1] Chen Song,[1] and Yang E-Chuan[1]

[1] *College of Mechanical Engineering, Chongqing University of Technology, Chongqing 400054, China*
[2] *Key Laboratory of Manufacture and Test Techniques for Automobile Parts, Ministry of Education, Chongqing 400054, China*

Correspondence should be addressed to Ding Jun; dingjunawen@126.com

Received 8 July 2014; Accepted 26 July 2014; Published 21 August 2014

Academic Editor: Xing Chen

This paper reports a numerical simulation procedure to model crack propagation in TGO layer and TGO growth near a surface groove in metal substrate upon multiple thermal-mechanical cycles. The material property change method is employed to model TGO formation cycle by cycle, and the creep properties for constituent materials are also incorporated. Two columns of repeated nodes are placed along the interface of the potential crack, and these nodes are bonded together as one node at a geometrical location. In terms of critical crack opening displacement criterion, onset of crack propagation in TGO layer has been determined by finite element analyses in comparison with that without predefined crack. Then, according to the results from the previous analyses, the input values for the critical failure parameters for the subsequent analyses can be decided. The robust capabilities of restart analysis in ABAQUS help to implement the overall simulation for TGO crack propagation. The comparison of the TGO final deformation profile between numerical and experimental observation shows a good agreement indicating the correctness and effectiveness of the present procedure, which can guide the prediction of the failure in TGO for the future design and optimization for TBC system.

1. Introduction

The continuous development in gas-turbine industry has pushed forward a more wide application of thermal barrier coatings (TBCs) to protect components exposed to extreme temperatures in gas-turbine blades. The benefit results from the remarkable ability to sustain high thermal gradients in the presence of adequate back-side cooling. A typical TBC system consists of four layers: the columnar TBC (usually made of ceramic coating), thermally grown oxide (TGO, commonly alumina), bond coat layer (BC), and the underlying superalloy substrate [1–3]. However, the durability and reliability issues limit its application as a prime-reliant material. Consequently, the thorough understanding of TBC failure mechanism is of considerable practical importance to the design of TBC system. Premature failures observed in a TBC system, such as TGO rumpling activated by the unevenness of the interface between TBC and BC layers [4], TBC crack induced by the brittleness and weaker adhesion between ceramic and substrate material, TBC separation caused by the rather bigger impurities existed at the interface [5], and TGO itself cracks resulted from the higher TGO growth stress [6], often occur in TBC system with the presence of grooves on the surface of the bond coats. These failures are mainly attributable to the morphology instability near a surface groove which is in turn caused by the substantial stress generated in TGO layer, resulting in crack formation and growth along the interface. Eventually, cracks from neighboring sites coalesce with each other, leading to a large-scale separation of the top coat layer [7]. Such phenomena could be more prominent when TBC experiences a more complicated loading condition, since turbine blade usually suffers not only thermal cycling but also mechanical loading at a high temperature due to the centrifugal force generated

by high speed revolution in operation. The mechanical loads may cause additional deformation, which could, in turn, accelerate the failure of the TBC system.

Recently, numerous researches have been performed to improve the durability and stability of TBC system by a deep investigation on displacement instability near surface groove and to probe the source of generation of higher-level stress in TGO layer. Evans et al. [8] reviewed the mechanism controlling the durability of TBC and pointed out that the failure of the system was ultimately connected to large residual compression developed in TGO layer. Karlsson et al. [9] had proposed a fundamental model to deeply explore the cyclic morphological instability occurred in TBC by devising a spherically symmetric model that can be solved analytically. At the same time, they employed a numerical method for the first time to investigate the displacement instabilities for a sinusoidal undulation embedded into the bond coat. Ambrico et al. [10] further derived analytical results for stress distribution and plastic zone sizes to pursue a mechanics-based explanation for the evolution of undulations with multiple thermal cycles. Subsequently, Karlsson et al. [11–13] performed some systematic works to investigate the distortion occurring near a single groove subjected to thermal cycling using a numerical method. They performed a series of finite-element simulations, which revealed that TGO displacement was diminished by increasing the high-temperature strength of the underlying bond coat but increased with the strength of TGO and the curvature of the groove edge. However, their studies were limited by the fact that many material properties, such as yield strengths and oxide growth rates, were assumed or idealized rather than being based on experimental measurements.

A review for the previous literatures shows that no such works are found that investigate failure mechanism due to crack in TGO itself and that explore the effects of TGO crack propagation on the displacement instabilities near a surface groove. Only some works relate to TBC failure or delamination at the interface between TBC layer and metal substrate layer. He et al. [14] had analyzed and described the mechanism for the delamination of thermal barrier systems and found that the system fails by large-scale buckling due to large displacement instability. Chen et al. [15] introduced a new model to determine the normal stresses and shear stresses generated at the interface incorporating some imperfections, which results in delamination of TBC system. The mechanics governing crack coalescence and the consequent failure were also addressed in the analysis. Tzimas et al. [16] had investigated the failure mechanisms of TBC system by using thermomechanical fatigue test and FE analysis and found that the decrease of the applied mechanical strain and hence of the developed stresses led to the suppression of failure by bond coat cracking and activated delamination. Bhatnagar et al. [17] employed a parametric study to explore the damage initiation and propagation along the interface between TGO and top TBC layers. Begley and Wadley [18] developed a micromechanical model to explore the effect of metal layers upon delamination failure of TBCs driven by thickening of TGO. Because of the difficulty in numerically modeling the delamination of TBC, cohesive model was also put forward to explore the failure mechanism occurring in TBC system, such as [19], wherein a cohesive model was employed for the purpose of lifetime prediction and obtaining better results in comparison with experimental measurement and other analyses.

Actually, due to the substantially higher level of stress generated in TGO layer caused by thermal expansion misfit and TGO formation at a high temperature, some microcracks are susceptible to initiate and coalesce with each other resulting in macrocrack appearing in TGO layer. Upon multiple thermal cycling, especially coupled with mechanical load, those cracks would rapidly propagate along the fragile interface and eventually lead to the failure of TBC system. However, only one work performed by Li et al. [20] showed experimental observation on TGO crack upon thermal cycling, and it was concluded that the displacement instability developed more severely under the thermomechanical loading history that mostly contributes to TGO crack itself. Although the research interests in TBC failure are growing, to the best of the authors' knowledge, any other additional experimental research has not been reported; this may be due to the technical difficulties of the experiments. Similarly, the research aiming at exploration on TGO crack propagation in TBC system has also never been found in reviews.

In this work, the initiation and propagation of crack in TGO due to displacement instability of the surface groove in Fecralloy substrate, subjected to multiple thermomechanical loading cycles, have been studied using the finite element procedure. The material property change method is employed to model TGO formation cycle by cycle, and the creep properties for constituent materials are also incorporated. Based on the finite element procedure developed by ourselves, two columns of duplicated nodes are placed along the interface of the potential crack, two nodes of which are bonded together in advance as one node. In terms of critical crack opening displacement criterion, crack initiation has been determined by several finite element analyses in comparison with that without predefined crack. Then, according to the results from the previous few analyses, it can decide the critical input parameters for subsequent analyses. The capability of restart analysis in ABAQUS helps to implement the overall simulation for TGO crack propagation. The comparison of the final deformation profile made with the experimental observation shows a good agreement indicating the effectiveness and correctness of the present procedure.

2. Materials and Methods

2.1. The Description for Experiment

2.1.1. Material Choice. Since the material generally used as BC alloy in gas-turbine industry is not commercially available due to the important technology secret, another material Fecralloy (Fe72.8/Cr22/Al5/Zr0.09) heat resistant alloy has been chosen as the substrate of specimen because Fecralloy forms a uniform α-Al_2O_3 scale in the absence of voids at the interface between the oxide and alloy just as the BC alloy does in a TBC system, which cannot violate the essence of research to crack propagation upon loading cycles.

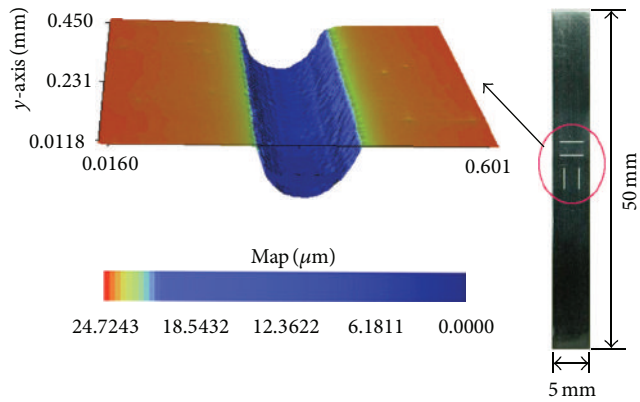

Figure 1: The geometry configuration of specimen and 3D surface profile at groove.

2.1.2. Specification of Specimen. The specimen has the rectangular shape with the dimension of ~5 mm × 50 mm × 0.5 mm. In order to investigate TGO failure more vividly, two groups of groove are made in the surface of Fecralloy substrate since the existence of the groove can enlarge TGO deformation near a surface groove due to displacement instability. One group of grooves aligned along the horizontal direction and the other group along the vertical direction are carved in the substrate surface by the precision machining center. Each group consists of two parallel grooves with the dimension of 20 ± 5 μm deep and 160 μm wide. To equilibrate the microstructure and eliminate residual stress, the specimens are annealed in a vacuum at 1100°C for 24 h. Thereafter, they are mechanically ground and polished to a 1 μm finish. A high accuracy noncontact surface profiler (NVC-10100, Nano-System Co., Ltd.) is used to measure the initial groove morphology. The geometry configuration and the alignment for the groves as well as the three-dimensional (3D) morphology of the groove are illustrated in Figure 1.

2.1.3. Experimental Observation. The specimens are then mounted on the microcreep tester for testing upon 24 thermal cycles. Each cycle consists of a 600 s cooling from 1200°C to the ambient, a 600 s heating, and 1800 s holding at high temperature. Meanwhile, the tensile stresses with the magnitude of 0.4, 0.8, and 1.2 MPa are applied on the both ends of the specimen only at the holding time, respectively. After testing, each specimen has been cut into foils for exposing the cross sections, then polished again, and examined by scanning electron microscopy (SEM).

Figure 2 illustrates the deformation shape near a surface groove and TGO crack observed in specimens. The white dotted line in the figure is the initial shape of the groove before experiment. It is evident that the greater upward deformation occurs at the periphery of the groove while the smaller one occurs at the base of the groove. In order to show the details for the deformation developed in TGO near surface groove, Figure 2(c) sketched the deformation profile at the periphery of the groove indicating that the deformation at the periphery groove seems much greater than that at the base of the groove. The drastic deformation in TGO at the periphery behaves upward, and the surrounding material cannot accommodate its deformation resulting in larger displacement instability in form of the arc segment. Figures 2(d) and 2(e) show that TGO crack occurring at the periphery of the groove is attributable to the high stresses in TGO due to its formation. Observation on the specimen indicates that cracks at the periphery of groove have penetrated through TGO thickness, but not entering into the underlying substrate material.

2.2. Numerical Simulation Procedure

2.2.1. Geometry and FEM Model. The experimental observation shows that TGO crack especially occurs at the periphery of the surface groove and at half section of groove due to the drastically displacement instability attributable to the misfit between CTE among various constituent materials and to the higher level of growth stress of TGO formation at the elevated temperature upon thermomechanical cycling. Although multiple cracks (usually at least two cracks) are found in TGO layer, because the emphasis in this work is put on simulation procedure on crack propagation along the crack surface, only one crack located at the periphery of surface groove is constructed in the model, and subsequent FE constructions are based on the single crack. Same procedure can work for the other cracks in TGO regardless of its location relative to surface groove.

Figures 3(a)~3(c) illustrate the modeling history simplifying from the actual specimen to FEM model. FEM model includes the full characteristic of crack in TGO and extracts half of the cross section (Figure 3(b)). Figure 3(e) shows the mesh used to discretize the model, which consists of 9936 quadrilateral, first-order generalized plane strain elements, CPEG4 in ABAQUS [21], with the number of the elements determined by the mesh dependency check of computation.

Regarding the details on the treatment for the crack, it will be separately discussed later. The description on boundary condition constrained is shown in Figure 3(d), wherein the nodes on the right side and on the bottom are allowed to move but the same displacement should be kept in x direction and y direction, respectively. Additionally, in order to restrict the rigid deformation, any one node in the model was chosen to be fixed in the y direction as well as x direction. Due to the application of mechanical load on the two ends of

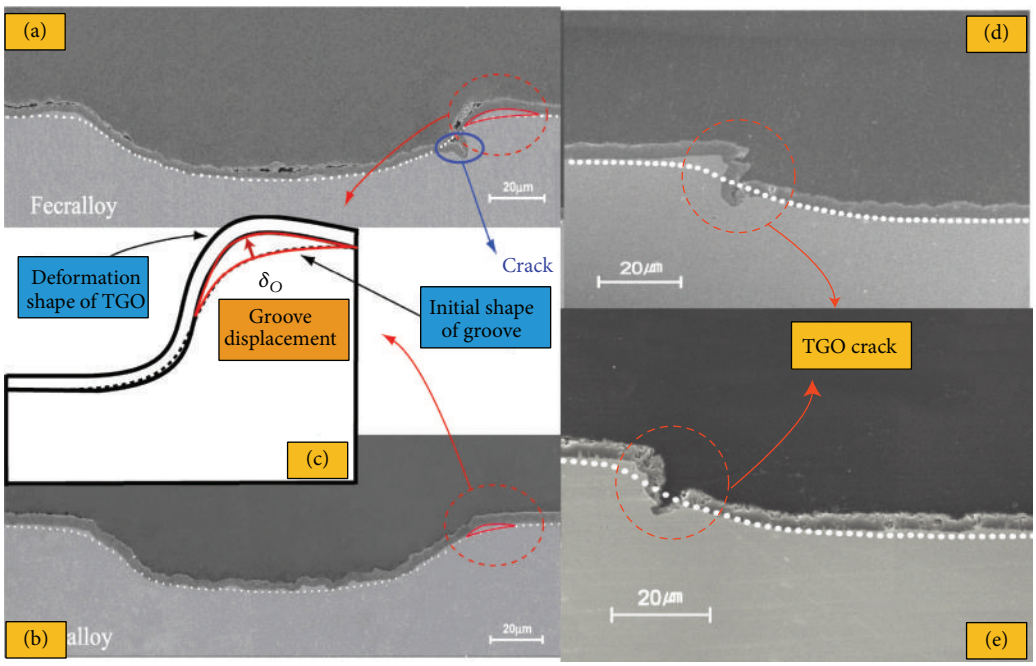

Figure 2: TGO crack and deformation shape near a surface groove.

Table 1: Material properties for TGO and metal substrate.

Material property	TGO	Metal substrate
Young's modulus (GPa)	390	140
Poisson's ratio	0.2	0.3
CTE (ppm/°C)	8.3	14.3
Creep exponent, n	2.0	2.5
Creep prefactor, A	$5.029e-11$	$3.903e-6$
Yielding stress, σ_y	At dwell time: $\sigma_y = 70$ MPa At cooling and heating: assumed to be elastic	$T < 300^\circ$C, $\sigma_y = 200$ MPa $T \geq 900^\circ$C, $\sigma_y = 7.6$ MPa σ_y vary linearly in between

the specimen with the magnitude of 0.4 MPa, 0.8 MPa, and 1.2 MPa, respectively, the tensile stress loading conditions are also applied in FEM in terms of pressure on the elements of end surface.

Since the specimen was subjected to the coupling load condition of thermal and mechanical cycling load, the treatment for load in FEA refers to the following, as shown in Figure 4. The cycle consists of a 600 s cooling from 1200°C to ambient, a 600 s reheating, and 1800 s holding at high temperatures. At the same time, mechanical load was applied at the two ends of specimen, but it keeps zero values during the periods of cooling and reheating, while suddenly ramps to the different level only at the dwell time of high temperature. It repeats until twenty-four cycles and synchronizes with the thermal cycling load.

2.2.2. Material Properties Used in FEA. As stated previously, one of the obvious limitations of previous works [9, 11–13] is the wide application of hypothesis material properties in FEA, resulting in full understanding for the ideal model but not adequate for the really physical phenomenon. The material parameters used in this work are obtained from in-house experimental measurement [22] and are summarized in Table 1.

Except for the conventional material properties such as elastic modulus and Poisson's ratio, a different property of creep behavior from our previous work has been taken into account in this work. In terms of loading history in experiment, the creep strain only occurs at the dwell time at high temperature by virtue of the fact that the mechanical load only is applied at that period resulting in the obvious creep deformation developed in the alloy specimens.

TGO and substrate are taken to have elastic-perfectly plastic material behavior. During one typical thermal cycling, TGO yielded at the elevated temperature (1200°C) when induced stress exceeded 70 MPa, whereas upon cooling and reheating it behaves elastically. For the metal substrate, the yield strength up to a temperature of 300°C was 200 MPa, and the yield strength is 7.6 MPa at temperatures above 900°C.

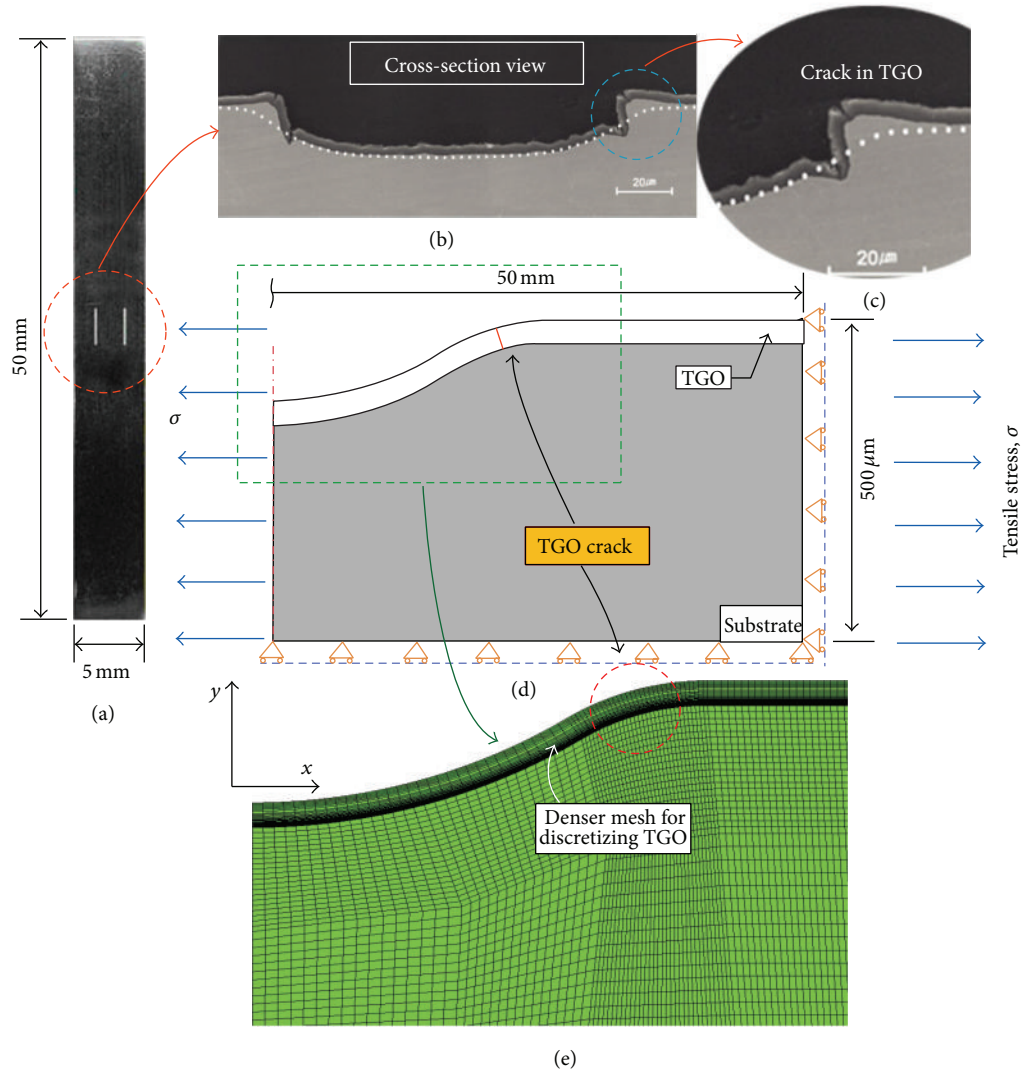

Figure 3: The modeling history and FEM model: (a) the rectangular specimen. (b) The cross-section view for the specimen. (c) The amplified view for the crack in TGO. (d) The boundary condition for FEM model. (f) The mesh for FEM model.

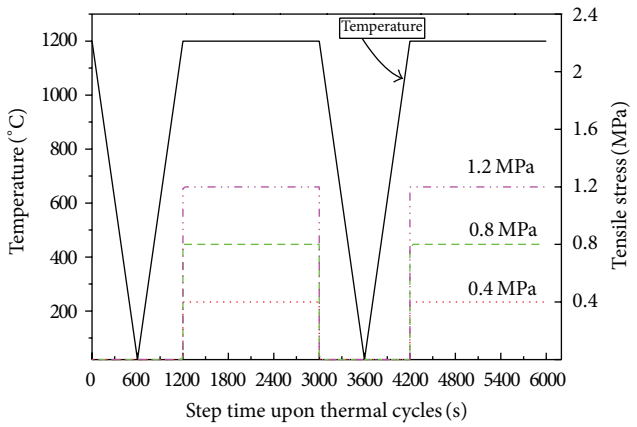

Figure 4: The temperature and mechanical load sequence upon thermal cycles.

For the intermediate temperatures, the yield strength is assumed to be linearly decreasing with temperature. Referring to our previous work [6], observation from the relation of TGO stress against strain shows that when TGO thickens to about 3 μm the ultimate tensile stress for TGO is about 92 MPa. Although TGO is taken in this work as elastic-perfectly plastic material, it actually behaves much more brittle than the neighboring substrate and indeed behaves as brittle material, especially upon cooling and reheating phases.

2.3. TGO Growth and Simulation Procedure. When holding at high temperature, TGO grows in two directions. The growth parallel to the interface contributes to the elongation or contraction of TGO, denoted by lateral growth, while that normal to the interface thickens the TGO, denoted by thickness growth. TGO lateral growth can be simulated by

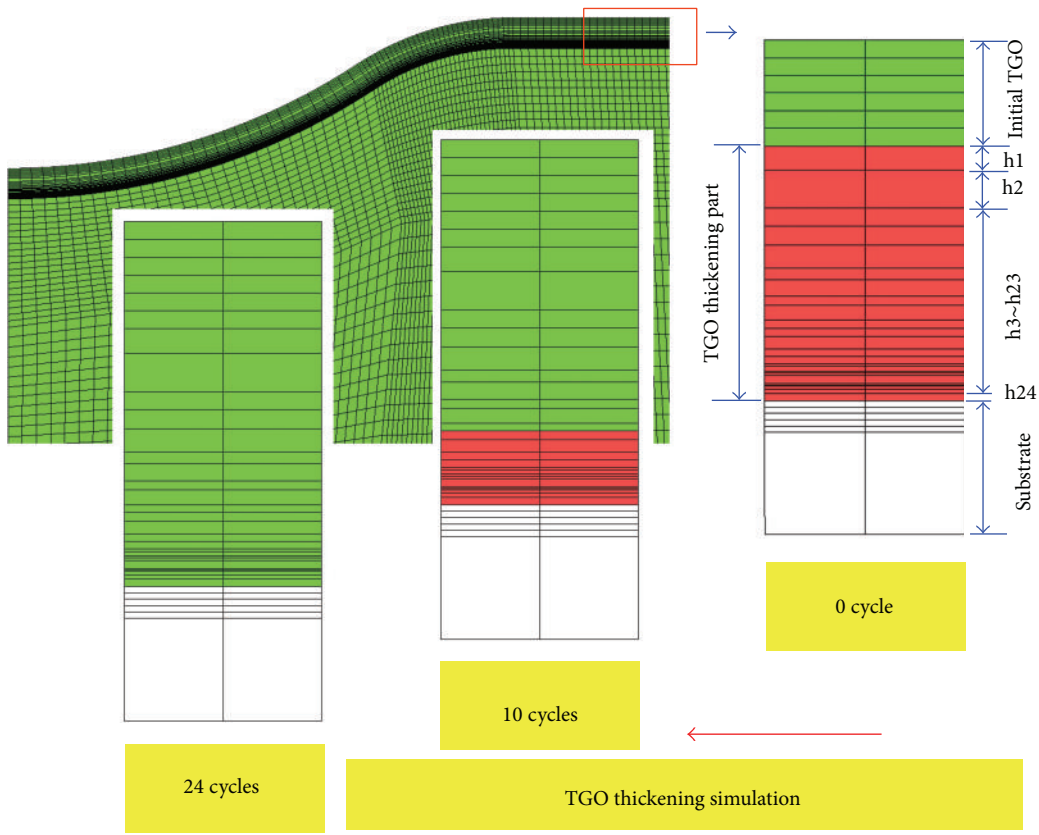

Figure 5: The sketch illustrating the TGO increasingly formed upon twenty-four thermal cycles.

the user subroutine, *UEXPAN*, which is a user subroutine used to define incremental thermal strain by user code in ABAQUS. It differs markedly with the previous simulation methods [8–13] since the actual thickness of TGO, which was formed in each cycle, was considered instead of the TGO thickening strain. It could not only eliminate the restriction of previous methods but also have the full capacity of simulating the displacement instability of TGO for the large TGO thickness other than the smaller one. The details have been already described in our previous work [6, 7].

The process of TGO growth in thickness could be simulated here by a method of material property change, which can model the successive formation of TGO from substrate material. It can be materialized by using the capability of user subroutine, *USDFLD*, which can be used to redefine the field variable at a material point by user code in ABAQUS software. The whole model can be divided into initial TGO, TGO thickening, and substrate layer in terms of thickness of TGO. TGO thickening layer, which is in essence different from initial TGO, represents that alumina which are produced from Fecralloy substrate through chemical interaction, while the initial TGO has already existed prior to the onset of thermal oxidation. TGO thickening layer was meshed into twenty-four sublayers, h1, h2~h24, with each layer representing a thickness of TGO formed in one respective thermal cycle, as sketched in Figure 5.

Prior to the implementation of analysis, the TGO thickening part was assigned to have substrate property. A newly introduced variable, *SDV* (solution dependent variable), in ABAQUS appearing in the subroutine code was used to control over the material property change from substrate to TGO. Namely, in the first thermal cycle, the uppermost sublayer of TGO thickening layer changes its material property to TGO by controlling the value of *SDV* to indicate the formation of new alumina. Afterwards, this layer keeps having TGO property. The same procedure was repeated for the next cycle, as shown in Figure 8. The occurrence of creep effects coincides with the formation of TGO. Since the creep parameters for TGO and substrate differ significantly, when the material property was changed from substrate to TGO, the change of the corresponding creep parameters synchronized automatically with the aid of the *SDV*.

2.4. The Mesh Treatment for TGO Crack. In compliance with the capability simulating crack propagation in ABAQUS, the crack should be predefined in construction of FEM model and the crack propagate along the predefined extend path. It requires that the user makes some special treatment for the crack definition and propagation direction along which crack propagates in simulation.

Figure 6 shows the details for the mesh at the crack in simulation procedure. The crack location is determined

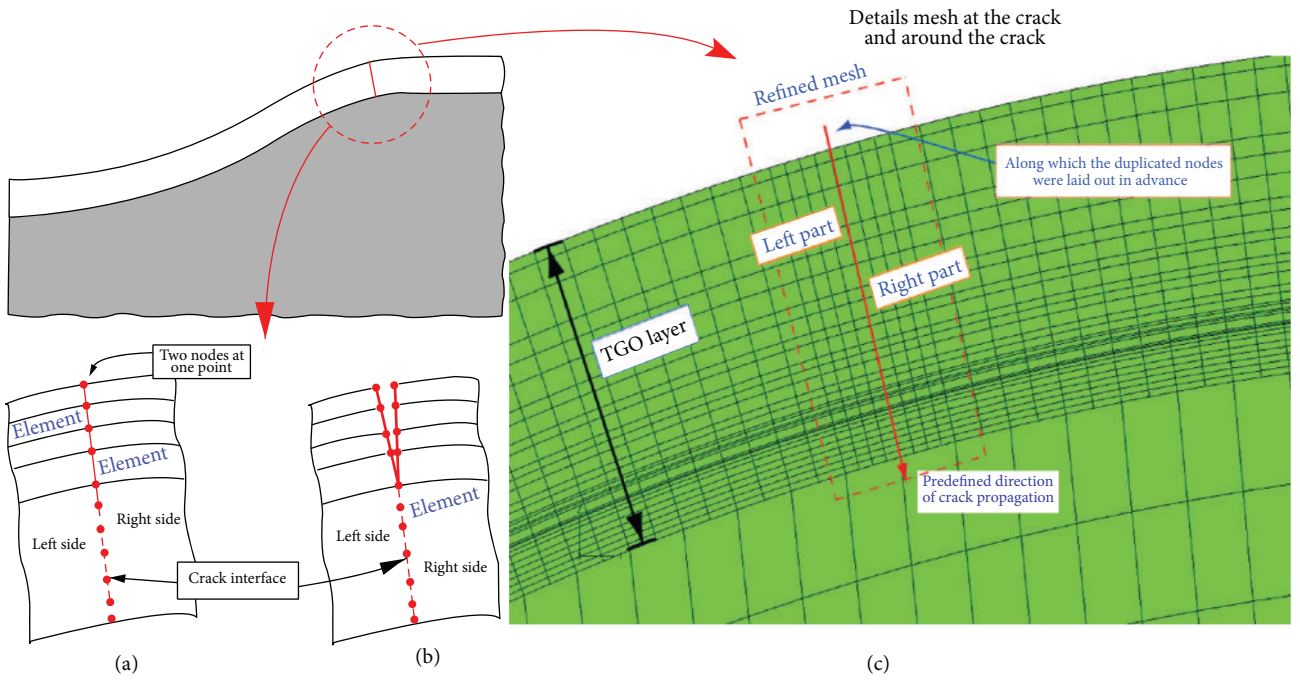

Figure 6: The crack model and the detail mesh at the crack.

in accordance with experimental measurement. And it is actually a through crack penetrating all of TGO thickness. Consequently, when constructing FEM model, the crack is predefined at the location in advance in the form of a slim seam. Figure 6(c) illustrates the detail mesh configuration around the crack. Two columns of double duplicated nodes are seeded along the seam line to represent the existence of the crack and as the potential propagation direction. That is, at the interface of crack, one FEM node incorporates two geometrical points and is assigned two node numbers, as shown in Figure 6(a). These two nodes are, firstly, bonded together in advance before running analysis using **TIE* command in ABAQUS. Once the employed failure criterion is reached, the corresponding nodes prior to this one should be released automatically and form a crack to propagate, as shown in Figure 6(b). Note in Figure 6(c) that the red line directed from the outer of groove toward the inner of groove represents the propagation direction along which crack propagates. The more refined elements are used to discretize the area around the crack seam to improve the accuracy of FEM simulation. The left part and the right part elements appeared in Figure 6(c) are employed for contact definition in simulation.

Figure 7 shows more details on FEM treatment for the predefined crack and its propagation direction, which is the amplified sketch for Figure 6(c). In the process of simulating crack propagation, the determination for node set in which these nodes will debond once criterion is reached is very important when constructing FEM model. The red line in Figure 7 is the predefined direction for crack propagation along which the duplicated nodes are generated at the same geometrical point. That is, nodes 53 and 54 share one geometrical point, while nodes 184 and 185 share one point. The number of node ranging from 53 to 3197 with the increment of 131 is considered as the node set required by the fracture criterion, indicating that those nodes will debond in a thermal cycle to model crack propagation. However, based on such an idea, ABAQUS can identify node 3197 as the target crack tip rather than node 53, which will result in crack propagation from the inner TGO to the outer TGO layer, on contrary to what we expected. To avoid the occurrence of this case, we suppose that a small initial crack exists in the initial TGO layer prior to the simulation. Consequently, the node set contains nodes beginning from node 184, rather than 53, to the node 3197. A verification for FEA shows that based on such definition of a node set ABAQUS successfully finds the target crack tip, node 184.

2.5. The Criterion for Crack Propagation. In order to simulate crack propagation in TGO, critical crack opening displacement criterion (CCOD) will be employed to model TGO crack propagation upon loading cycles. Since the crack appears in the form of a seam, it indeed has two crack surfaces but these surfaces contact closely before simulation. To avoid drastic nonlinearity due to these surfaces, the master and slave contact surfaces should be defined for the left and right part (Figure 6(c)), respectively. For the convenience of identifying the location of a crack tip, in addition to definition for the slave and master surfaces, the determination for the node set that marks the boundary reached by CCOD criterion is very important. If the node set is not specified, the initial contact conditions apply to the entire contact pair, and no crack tips can be identified. Thus, the bonded surfaces will not separate and the simulation for crack propagation fails.

Figure 7: The definition for node set for contact definition.

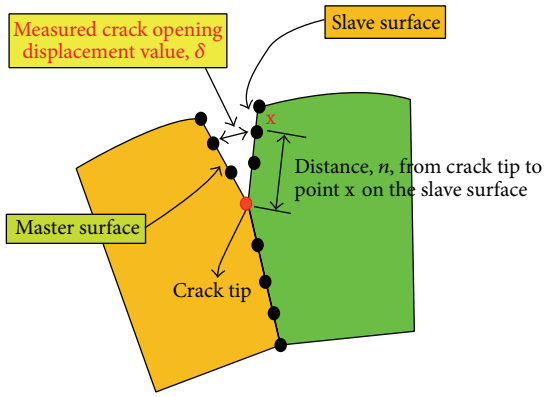

Figure 8: Sketch for the distance specification in CCOD.

Once the node set is defined, the initial contact condition applies only for the surfaces associated with the node set. The surfaces are assumed to be initially bonded within the length that the node set covers to construct the initial contact condition. ABAQUS will check ensuring that the defined node set includes only slave nodes belonging to the specified contact pair and separate two bonded surfaces according to CCOD criterion.

The required parameters for crack propagation are illustrated in Figure 8. The distance, n, is measured along the straight line connecting the current crack tip and the point behind the crack tip at which the crack opening displacement is calculated. The crack opening displacement, δ, represents the value measured at the point of the distance, δ, behind the crack tip. ABAQUS automatically calculates this value and compares it with the critical crack opening displacement given by the user to determine whether the crack-tip nodes specified in node set.

Once the value $f = \delta/\delta_c$ for attaining 1.0, the node at a crack tip should debond to model the crack propagation. The implementation can be performed by the ABAQUS command *FRACTURE CRITERION. In addition to distance, n, and the critical crack opening displacement, δ_c, the cumulative crack length should also be specified that is dynamically measured along the slave surface in the current configuration between the initial and the current crack tip, as illustrated in Figure 9.

3. Results and Discussion

3.1. The Determination for Onset of Crack Propagation. In terms of the simulation procedure as described previously, a series of finite element analyses had been performed to investigate the mechanical behavior of TGO crack propagation. In order to simulate the subsequent TGO crack propagation upon twenty-four thermal mechanical loading cycles, it is important to determine the time of onset of crack propagation. Although Figure 7 indicates that the initial crack tip is supposed as node 184 (same as 185 since they are coincided together) at the initial of simulation, it is difficult to decide the specific time of crack initiation. To decide the time of crack initiation, several times of finite element analyses were conducted as follows. Suppose that crack will propagate in the first loading cycle and input the corresponding values for n, δ_c, and critical COD, as explained in Figure 9, in ABAQUS keywords *FRACTURE CRITERION, and then

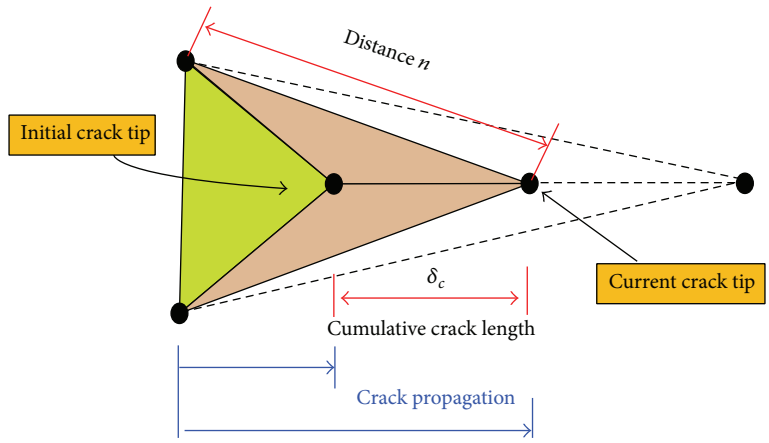

FIGURE 9: The definition of δ_c and crack propagation.

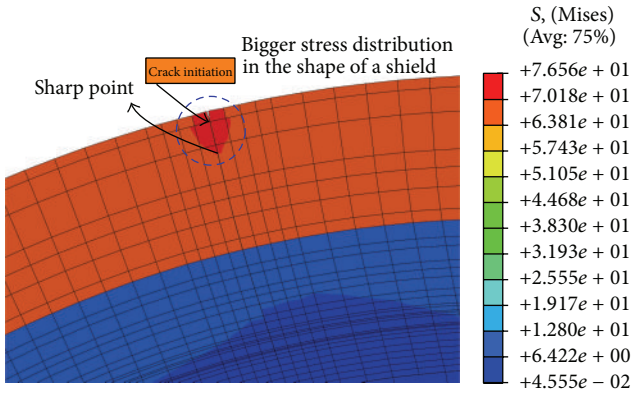

FIGURE 10: The Von-Mises stress distribution at the periphery of surface groove.

run the analysis. Once the analysis is completed, the final deformation profile after one loading cycle is compared with that from case without predefined crack. If no difference in profile has been observed, especially at the periphery of the surface groove since the drastic deformation develops at this site, it concluded that no crack initiates and propagates. It repeats until the sixth loading cycles. The comparison for the deformation profile at the periphery of surface groove shows the difference, and the cracked case illustrates bigger crack at the site. More investigation to the analysis file implies that the TGO crack is initiated at the cooling phase in the sixth cycle. Figure 10 shows the Von-Mises stress distribution for the sixth loading cycle and it can be found that a bigger stress distribution appears across four elements while the center line located at the four elements is just the predefined crack line. The bigger stress distribution looks like a shape of shield, and the sharp point located at the downward shield shape is just node 315, the location of a crack tip at the present analysis step. Obvious crack propagation for the initiated crack is observed in the figure implying onset of the crack advance.

3.2. TGO Growth upon Cycles. An important feature for the numerical simulation procedure in this work is to simulate TGO growth upon loading cycle with crack propagation, which is an actual physical phenomenon from metal substrate material to TGO material. The details for the simulation scheme have already discussed in Section 2.3 at full length. The main purpose in this section is to illustrate the actual realization of TGO growth in the simulation scheme.

Figure 11 shows the successful material transition from the metal substrate to TGO material in typical loading cycles. For the convenience of describing the fact, the results from the fourth, the sixth, the seventh, and the eighth loading cycle, corresponding to Figures 11(a)–11(d), respectively, are chosen to show the consecutive growth of TGO upon loading cycles. Note in Figure 11 that the red area represents the formed TGO and the blue color represents the metal substrate and that the first layer in Figure 11 is the initial TGO layer. Figure 11(a) means that only four layers of TGO were formed (same to TGO growth) in four cycles, Figure 11(b) six layers of TGO formed, Figure 11(c) seven layers of TGO formed, and Figure 11(d) eight layers of TGO formed, all of which are the manifest as the successful simulation of TGO growth upon loading cycles. At the same time, note also that TGO crack propagation occurs simultaneously with TGO growth from no crack (Figure 11(a)), crack initiation (Figure 11(b)), to crack propagation along the interface (Figure 11(d)).

Figure 12 shows the comparison of Von-Mises stress in two elements, one located in the initial TGO layer and the other in the first layer of TGO (being actual metal substrate material before the first thermal cycle), upon the previous eight loading cycles. The first layer of TGO is expected to change into TGO material property from the substrate in the first thermal cycle and retain TGO material property until the end of thermal cycles. It is evident from the figure that in the first thermal cycle, the Von-Mises stress distribution differs in the two elements, and the stress in the first layer of TGO is much smaller than that for the initial TGO part because at the moment the overall TGO thickening part consists of only substrate, much softer than TGO. However, from the

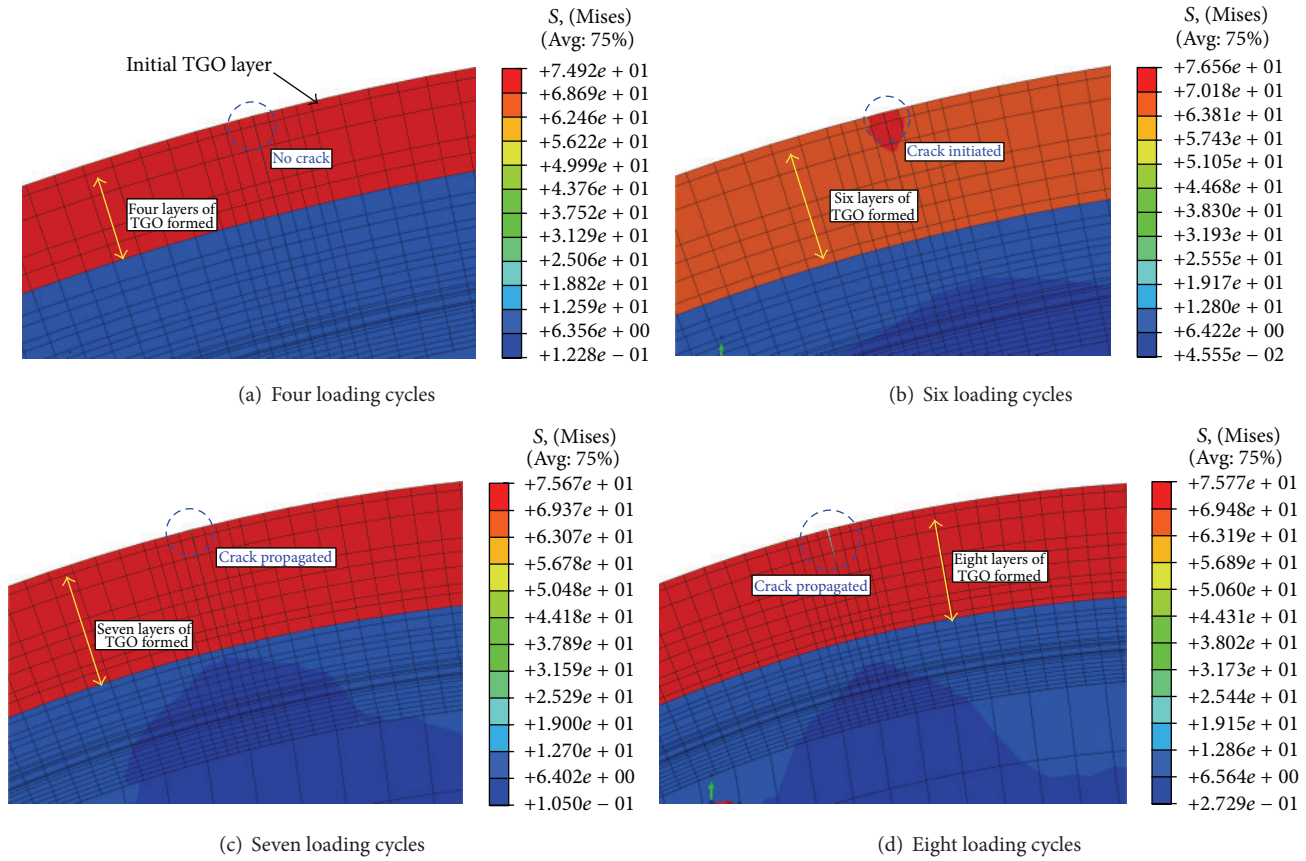

Figure 11: TGO growth upon cycles with TGO crack propagation: (a) 4 loading cycles, (b) 6 loading cycles, (c) 7 loading cycles, and (d) 8 loading cycles.

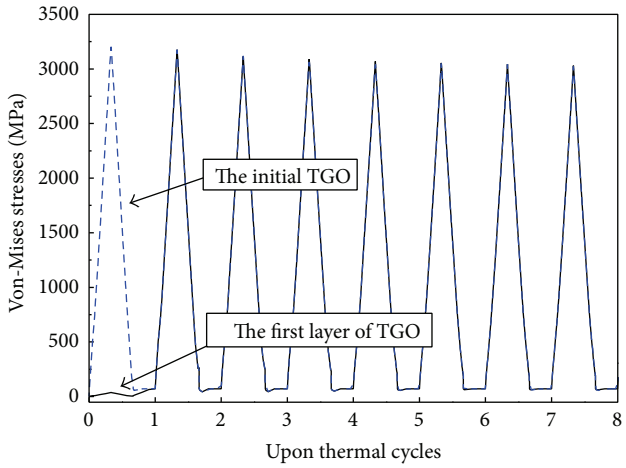

Figure 12: The variation of Von-Mises stress in the initial TGO and in the first layer of TGO with the previous eight cycles.

second thermal cycle, the Von-Mises stress curves for two elements coincide completely with each other implying that this layer of substrate material has already transformed into TGO.

3.3. Crack Propagation till 24 Cycles. Although the criterion used for simulating TGO crack propagation and the corresponding parameters for the CCOD are separately described in Section 2.5, the specific determination for the detailed input parameters with respect to some loading cycles deserves to be discussed. Figure 13 shows the parameters including distance, cumulative crack length, and the critical COD in the TGO deformation profile in the sixth loading cycle but for the input ready for simulating crack propagation occurring in the seventh and eighth loading cycles. Referring to the previous calculation (Section 3.1), it can be known that a new crack is formed and propagates at a very small distance in the sixth loading cycle. The investigation to the data file produced by ABAQUS execution shows that the present crack tip is at nodes 184 and 185, as illustrated in Figure 13. In terms of the physical meaning of the input parameters, in order for crack to propagate in the seventh loading cycle, the distance, the critical COD, and the cumulative crack length should be 9.5e-5, 3.9e-6, and 2.32e-4 mm, respectively. The distance n equals approximately to the length of the initial TGO layer, 1e-4 mm. The reason for its value being used less than the actual thickness is that the location at which the COD is measured somewhat deviates from the outer node of the groove surface.

Based on the numerical simulation procedure, finite element analyses have been performed until twenty-four

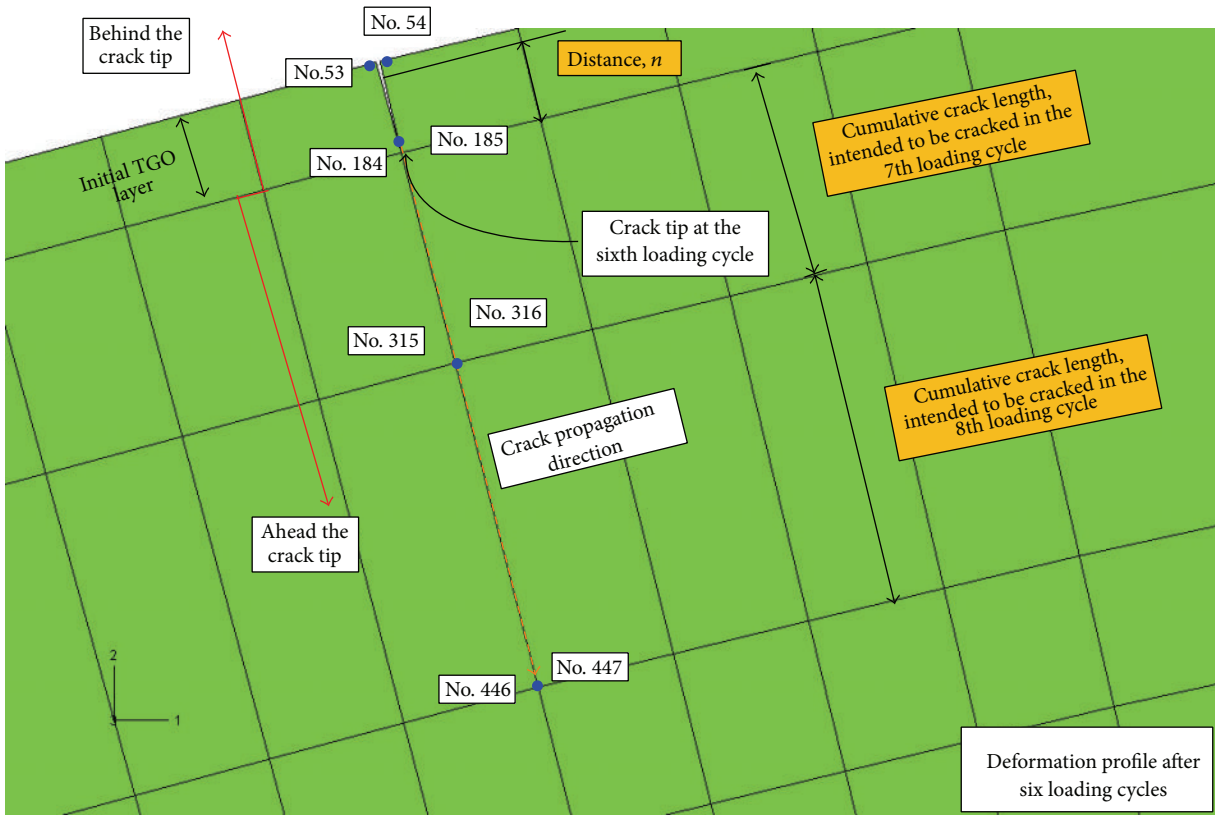

Figure 13: The determination to input parameters of CCOD for simulating crack propagation after six loading cycles.

loading cycles to simulate TGO crack propagation. Figures 14(a)–14(f) illustrate the TGO final deformation profile for 4 loading cycles, 8 loading cycles, 12 loading cycles, 16 loading cycles, 20 loading cycles, and 24 loading cycles, respectively. Note in the figure that no crack propagation was observed in the 4 loading cycles except for the predefined crack since the onset of crack propagation firstly occurs in the sixth loading cycle and, at the same time, small displacement instability was not also observed in this case. However, crack propagation happens in the 6th loading cycle and it continues to extend along the interface, and the COD for crack becomes wider, as illustrated in Figure 14(b). And the upward deformation at the periphery of groove seems more obvious than that for the fourth loading cycle, as a proof of displacement instability. As loading cycle proceeds, crack in TGO layer continues to propagate and COD at the crack becomes wider and wider. Since the predefined TGO crack is just located at the convex point of the groove, it is much easier to deform outward that other node in this area. As the loading cycle continues, the accumulated deformation at this site and the wider COD at the crack make the periphery near the surface groove more compliance, and it can be susceptible to deform outward resulting in drastic upward deformation at the periphery. When at 24 loading cycles, such deformation becomes serious, and it forms an obvious upward deformation at the site, as illustrated in Figure 14(f).

Figure 15 shows a comparison of TGO final deformation between numerical and experiment results. Due to the geometrical symmetry, half specimen and half deformation profile have been chosen for comparison. The white dots and the black fine dashed line indicate the initial cross-sectional shapes of a groove in an experimental specimen and in the numerical model, respectively. The two parallel red solid lines indicate the final deformation shape of TGO near the groove in the model after 24 thermomechanical cycling. The solid part between two red lines represents TGO formed after twenty-four loading cycles, which can almost be equal in thickness to actual TGO from experimental measurement, further proving that the procedure to simulate TGO growth is accurate. A focus has been placed on TGO crack between them implying that numerical simulation result can capture the essence of TGO crack propagation happening in experiment measurement. The tendencies of crack extending between them remain consistent, and the deformation at other segments of TGO agrees well with each other, which shows the validity and the accuracy of the finite element procedure. A slight discrepancy was found on COD (crack opening displacement) at the crack at the periphery of groove. The COD for experiment looks larger than that from FEA results. It can be explained as follows. In reality, TGO is formed cycle by cycle, and it becomes thicker and thicker, leading to a much more brittle and behaves more rigid when it thickens. Once TGO crack

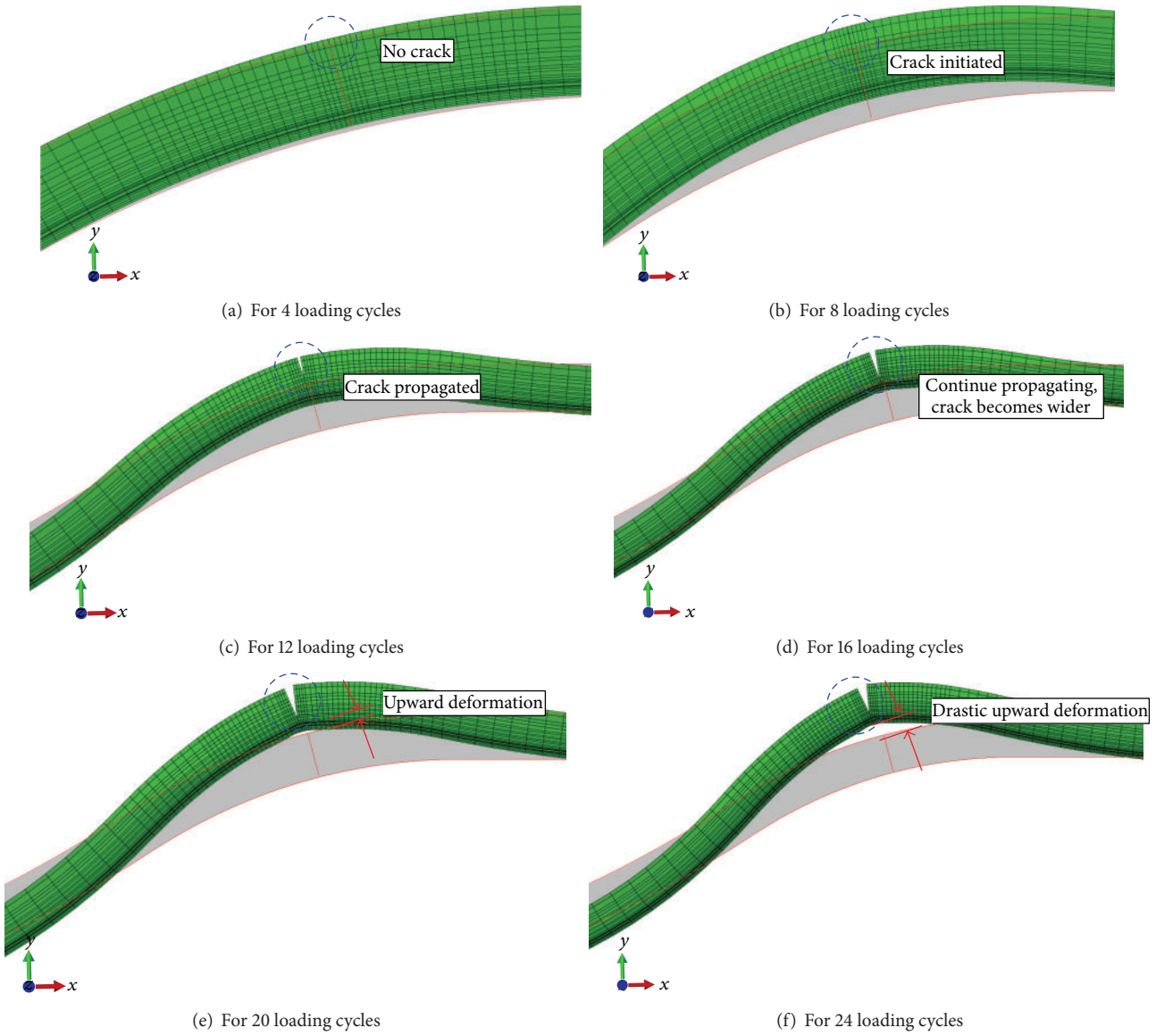

(a) For 4 loading cycles

(b) For 8 loading cycles

(c) For 12 loading cycles

(d) For 16 loading cycles

(e) For 20 loading cycles

(f) For 24 loading cycles

Figure 14: TGO deformation indicating crack propagation upon twenty-four loading cycles: (a) for 4 loading cycles, (b) for 8 loading cycles, (c) for 12 loading cycles, (d) for 16 loading cycles, (e) for 20 loading cycles, and (f) for 24 loading cycles.

propagates in experiment, it will be more susceptible to crack due to its more brittle. However, in FEA simulation, the brittleness for TGO remains constant regardless of its thickness, and TGO crack propagation remains steady. The numerical result slightly underestimated the amount of deformations around the crack in comparison with the experiment observation. The further research on it hopes to improve the result.

4. Conclusions

A series of finite element analyses had been performed to simulate TGO crack propagation upon loading cycles, which take accounts of TGO growth. The finite element analyses have used in-house measured material parameters as many as possible with the assumption of material properties to be minimized. Consequently, a quantitatively good agreement with the experiment has been achieved. A special technique is used to simulate TGO thickening and the CCOD criterion used to determine the onset of crack propagation and its subsequent extension along the predefined propagation path. The comparison of the TGO final deformation profile made with the experimental observation shows a good agreement indicating the correctness and effectiveness of the present procedure, which can guide the prediction of the failure in TGO for the future design and optimization for TBC system.

Conflict of Interests

The authors declare no conflict of interests.

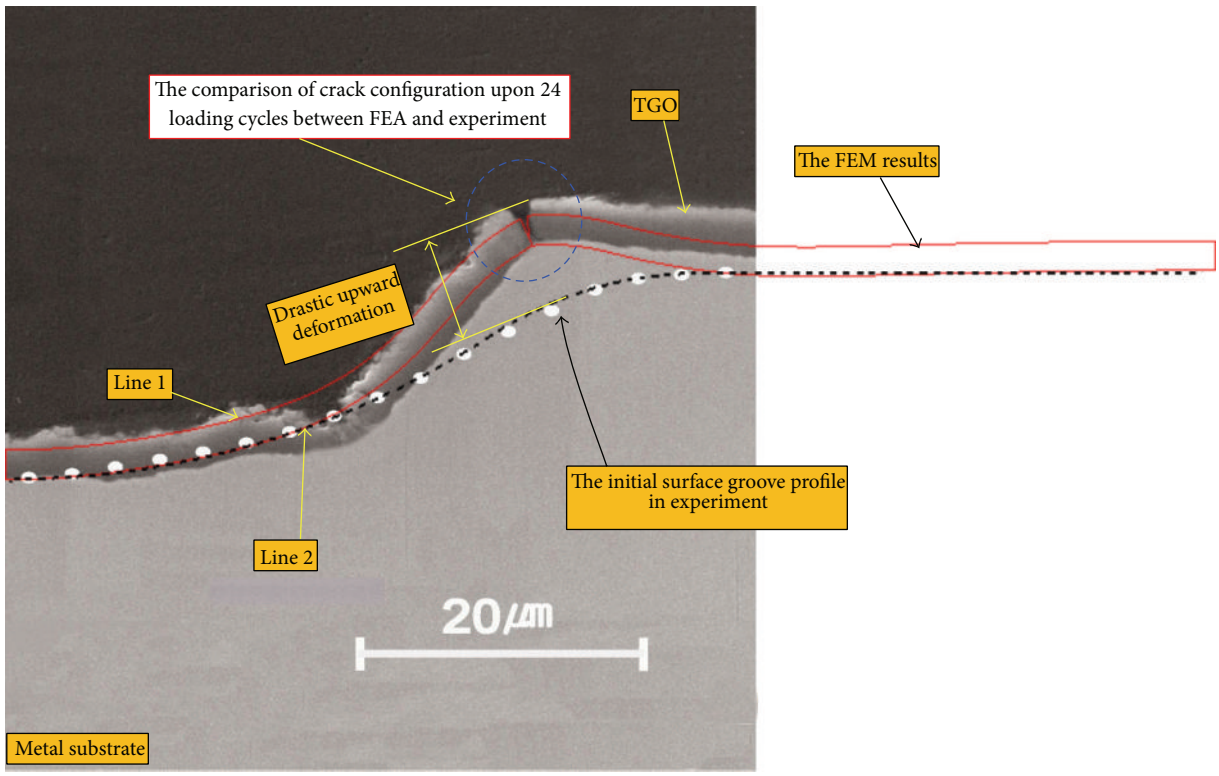

Figure 15: The comparison of TGO final deformation profile between FEA result and experimental observation.

Acknowledgments

This work is financially supported by the Natural Science Foundation of China (11302272), by the Natural Science Foundation of China (11272368), by the 2013 Program for Innovation Team Building at Institutions of Higher Education in Chongqing (KJTD201319), and by the Science and Technology Project Affiliated with the Education Department of Chongqing Municipality (KJ120801).

References

[1] A. G. Evans, D. R. Mumm, J. W. Hutchinson, G. H. Meier, and F. S. Pettit, "Mechanisms controlling the durability of thermal barrier coatings," *Progress in Materials Science*, vol. 46, no. 5, pp. 505–553, 2001.

[2] R. Rajendran, "Gas turbine coatings—an overview," *Engineering Failure Analysis*, vol. 26, pp. 355–369, 2012.

[3] D. S. Balint, T. Xu, J. W. Hutchinson, and A. G. Evans, "Influence of bond coat thickness on the cyclic rumpling of thermally grown oxides," *Acta Materialia*, vol. 54, no. 7, pp. 1815–1820, 2006.

[4] V. K. Tolpygo and D. R. Clarke, "Alumina scale failure resulting from stress relaxation," *Surface and Coatings Technology*, vol. 120-121, pp. 1–7, 1999.

[5] V. K. Tolpygo and D. R. Clarke, "Tensile cracking during thermal cycling of alumina films formed by high-temperature oxidation," *Acta Materialia*, vol. 47, no. 13, pp. 3589–3605, 1999.

[6] J. Ding, F. Li, and K. Kang, "Numerical simulation of displacement instabilities of surface grooves on an alumina forming alloy during thermal cycling oxidation," *Journal of Mechanical Science and Technology*, vol. 23, no. 8, pp. 2308–2319, 2009.

[7] J. Ding, F. Li, and K. Kang, "Effects of material creep on displacement instability in a surface groove under thermo-mechanical cycling," *Surface and Coatings Technology*, vol. 204, no. 1-2, pp. 157–164, 2009.

[8] A. G. Evans, M. Y. He, A. Suzuki, M. Gigliotti, B. Hazel, and T. M. Pollock, "A mechanism governing oxidation-assisted low-cycle fatigue of superalloys," *Acta Materialia*, vol. 57, no. 10, pp. 2969–2983, 2009.

[9] A. M. Karlsson, J. W. Hutchinson, and A. G. Evans, "A fundamental model of cyclic instabilities in thermal barrier systems," *Journal of the Mechanics and Physics of Solids*, vol. 50, no. 8, pp. 1565–1589, 2002.

[10] J. M. Ambrico, M. R. Begley, and E. H. Jordan, "Stress and shape evolution of irregularities in oxide films on elastic-plastic substrates due to thermal cycling and film growth," *Acta Materialia*, vol. 49, no. 9, pp. 1577–1588, 2001.

[11] A. M. Karlsson and A. G. Evans, "A numerical model for the cyclic instability of thermally grown oxides in thermal barrier systems," *Acta Materialia*, vol. 49, no. 10, pp. 1793–1804, 2001.

[12] A. M. Karlsson, C. G. Levi, and A. G. Evans, "A model study of displacement instabilities during cyclic oxidation," *Acta Materialia*, vol. 50, no. 6, pp. 1263–1273, 2002.

[13] A. M. Karlsson, J. W. Hutchinson, and A. G. Evans, "The displacement of the thermally grown oxide in thermal barrier systems upon temperature cycling," *Materials Science and Engineering A*, vol. 351, no. 1-2, pp. 244–257, 2003.

[14] M. Y. He, D. R. Mumm, and A. G. Evans, "Criteria for the delamination of thermal barrier coatings: with application to

thermal gradients," *Surface and Coatings Technology*, vol. 185, no. 2-3, pp. 184–193, 2004.

[15] Z. X. Chen, Z. G. Wang, F. H. Yuan, and S. J. Zhu, "Interfacial fracture behavior of a thermal barrier coating system under four-point bend loading," *Materials Science and Engineering A*, vol. 483-484, no. 1-2, pp. 629–632, 2008.

[16] E. Tzimas, H. Müllejans, S. D. Peteves, J. Bressers, and W. Stamm, "Failure of thermal barrier coating systems under cyclic thermomechanical loading," *Acta Materialia*, vol. 48, no. 18-19, pp. 4699–4707, 2000.

[17] H. Bhatnagar, S. Ghosh, and M. E. Walter, "A parametric study of damage initiation and propagation in EB-PVD thermal barrier coatings," *Mechanics of Materials*, vol. 42, no. 1, pp. 96–107, 2010.

[18] M. R. Begley and H. N. G. Wadley, "Delamination resistance of thermal barrier coatings containing embedded ductile layers," *Acta Materialia*, vol. 60, no. 6-7, pp. 2497–2508, 2012.

[19] O. Nguyen, E. A. Repetto, M. Ortiz, and R. A. Radovitzky, "A cohesive model of fatigue crack growth," *International Journal of Fracture*, vol. 110, no. 4, pp. 351–369, 2001.

[20] F. Li, J. Ding, and K. Kang, "Morphological change occurring near a surface groove on an alumina-forming alloy subjected to thermal and mechanical cycling," *Surface and Coatings Technology*, vol. 204, no. 9-10, pp. 1461–1468, 2010.

[21] ABAQUS version 6.10, *User Documentation*, Dassault Systemes, 2010.

[22] G. D. Ko, *Thermally grown oxides formed on superalloy surfaces and their mechanical properties at high temperature [M.S. thesis]*, Chonnam National University, 2007.